JOURNAL OF MATERIALS SCIENCE 29 (1994) 2216–2230

# The probability of hertzian fracture

A. C. FISCHER-CRIPPS, R. E. COLLINS
*School of Physics, University of Sydney, New South Wales 2006, Australia*

The indentation strength of brittle solids is traditionally characterized by Auerbach's law, which predicts a linear relationship between the load required to initiate a Hertzian cone crack and the radius of a spherical indentor. This paper reviews both the energy balance and flaw statistical explanations of Auerbach's law. It is shown that Auerbach's law in the strictest sense only applies to well-abraded specimens. A novel application of Weibull statistics is presented which allows the distribution of fracture loads to be predicted for any specimen surface condition for a given indentor size. The indentation strength of a brittle solid, for both spherical and cylindrical indentors, is shown to be influenced by both its surface flaw statistics and the degree of interfacial friction. It is observed that the indentation strength of soda–lime glass is increased by a factor of about three times that expected for frictionless contact, and that for a fully bonded indentor, conical fractures cannot occur.

## 1. Introduction

Indentation fracture of glass was first studied in detail by Hertz [1, 2] in 1881. Hertz found that a cone crack of characteristic appearance occurred in a flat specimen of glass which was loaded by a hard, spherical indentor. The cone crack was observed to start near the edge of the contact circle where the tensile stresses in the specimen were calculated to be the greatest. In 1891, Auerbach [3] noted that the cone crack appeared when the force reached a critical value which is directly proportional to the radius of the indentor. The empirical linear relationship between this critical force and the radius of the indentor has become known as "Auerbach's law". Early analyses of this type of fracture appeared to indicate that Auerbach's law contradicts the Griffith energy balance criterion [4] for crack growth. Attempts were subsequently made to explain Auerbach's law in terms of the statistical spread of surface flaws in the specimen and quantitative analysis [5] appeared to show good correlation with experimental evidence. However, the statistical approach failed to account for several key features of the phenomenon. In 1967, Frank and Lawn [6] applied the Griffith fracture criterion so as to account for the way in which the tensile stress field rapidly decreases with depth into the specimen in the vicinity of the indentor. They argued that Auerbach's law is a consequence of the existence of a hitherto unobserved shallow ring crack which precedes the formation of the more familiar visible cone crack. In 1984, Mouginot and Maugis [7], in an important development of Frank and Lawn's work, showed that Auerbach's law could be explained, without reference to an initial ring crack, by including the effect of the starting radius of the crack in the energy balance method.

In the present paper, we briefly review the work of Mouginot and Maugis and then develop a method, using Weibull statistics [8], which allows a determination of the probability of occurrence of an indentation cone crack for a given load and specimen surface condition. We then review some of the published data for Hertzian fracture and present some experimental results for both spherical and cylindrical indentors. These data indicate that the frictional forces between the indentor and the specimen have a major influence on the stress fields which lead to indentation fracture, and that surface flaw statistics influence the probability of occurrence of such a fracture.

## 2. The Hertzian stress field

When a rigid cylindrical or spherical indentor is in frictionless contact with a flat surface of a solid, linear elastic analysis shows that on the surface of the specimen, beneath the indentor, all three principal stresses are compressive and all have approximately the same magnitude. Outside the contact circle, the $\sigma_1$ principal stress is a tensile radial stress and has a maximum value at the edge of the contact circle. It is this stress that causes the initiation of a cone crack. The hoop stress, $\sigma_2$, is compressive in this region, and on the surface, has a value approximately equal (but opposite in sign) to that of the radial tensile stress $\sigma_1$. The direction of the third principal stress, $\sigma_3$, at the surface is normal to the surface because, by definition, it is orthogonal to $\sigma_1$ and $\sigma_2$. The magnitude of $\sigma_3$ at the surface is, of course, zero outside the contact circle because it acts normal to a free surface in this region. It is convenient to label the stresses such that nearly always $\sigma_1 > \sigma_2 > \sigma_3$.

For points inside the specimen, the magnitude and direction of the three principal stresses change. The $\sigma_1$ stress decreases rapidly with increasing depth but remains tensile outside a drop-shaped compressive zone underneath the indentor. The $\sigma_2$ hoop stress



0022–2461 

remains compressive but with decreasing magnitude until at some depth in the material it becomes tensile. The so-called "normal stress", $\sigma_3$, is compressive for all points away from the surface and not directly below the indentor. Fig. 1 shows the contours of normalized principal stresses for an indentation stress field for the case of a flat punch cylindrical indentor. These contours were generated using the finite element method of analysis. In Fig. 1, the contours are normalized to the mean pressure beneath the indentor, and distances are expressed in terms of the indentor radius.

The important feature of the indentation stress field for the initiation of a conical fracture is the tensile region near the specimen surface just outside the area of contact. For brittle solids, Hertz noted that when the load on the indentor is sufficient, the characteristic cone crack which forms appears to start close to the circle of contact near where $\sigma_1$ is greatest and proceeds down and outwards approximately along the path of the $\sigma_3$ stress trajectory. The general features of a Hertzian cone crack are shown in Fig. 2.

Assuming linear elasticity throughout, Hertz found that for a spherical indentor, the radius of the circle of contact, $a$, is related to the indentor load, $P$, the indentor radius, $R$, and the elastic properties of the materials by

$$a^3 = \frac{3}{4}(1 - \nu^2)\frac{kPR}{E} \tag{1a}$$

where

$$k = 1 + \frac{(1 - \nu'^2)E}{(1 - \nu^2)E'} \tag{1b}$$

and $E$, $\nu$ and $E'$, $\nu'$ are the Young's modulus and Possion's ratio for the specimen and the indentor, respectively. For an indentor and specimen of the same material, $k = 2$; for a rigid indentor, $k = 1$.

Hertz also found that the maximum tensile stress in the specimen is radial and occurs at the edge of the contact circle at the surface. The magnitude of this maximum stress is

$$\sigma_{max} = (1 - 2\nu)\frac{P}{2\pi a^2} \tag{2}$$

The radial tensile stress on the surface outside the indentor decreases as the inverse square of the distance away from the centre of contact.

Combining Equations 1 and 2, the maximum tensile stress outside the indentor can be expressed in terms of the indentor radius, $R$

$$\sigma_{max} = \left[\frac{(1 - 2\nu)}{2\pi}\right]\left[\frac{4E}{3(1 - \nu^2)k}\right]^{2/3} P^{1/3}R^{-2/3} \tag{3}$$

Auerbach [3] found experimentally that, for a wide range of brittle materials, the force $P$ required to produce a cone crack is proportional to $R$ such that

$$P = AR \tag{4}$$

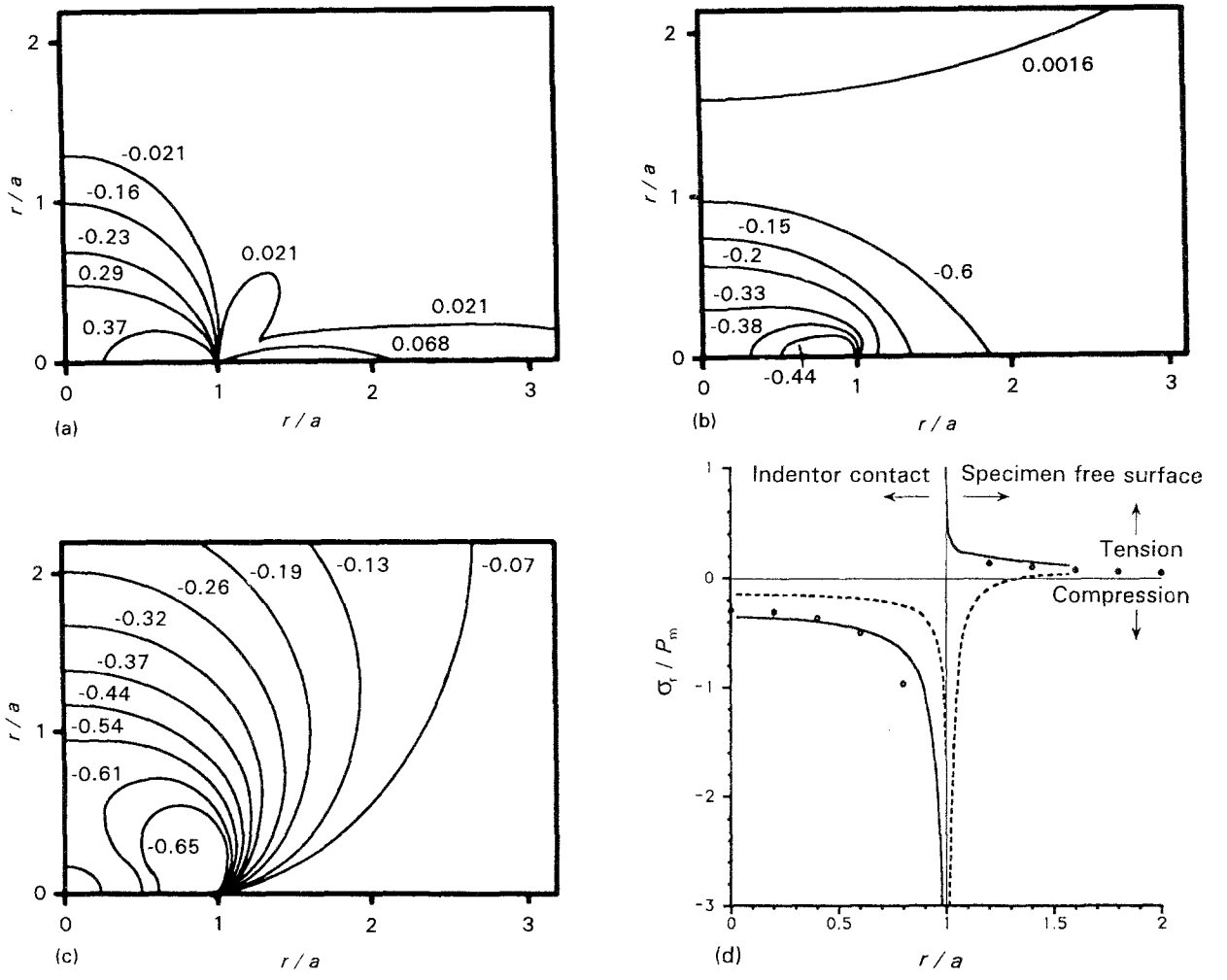


*Figure 1* Contours of constant stress generated by the finite element method for a cylindrical flat punch indentor. (a) $\sigma_1$, (b) $\sigma_2$, (c) $\sigma_3$. (d) The distribution of surface radial stress in the vicinity of the indentor for both (——) full slip and (——) no slip contact. (○) Sneddon [14].

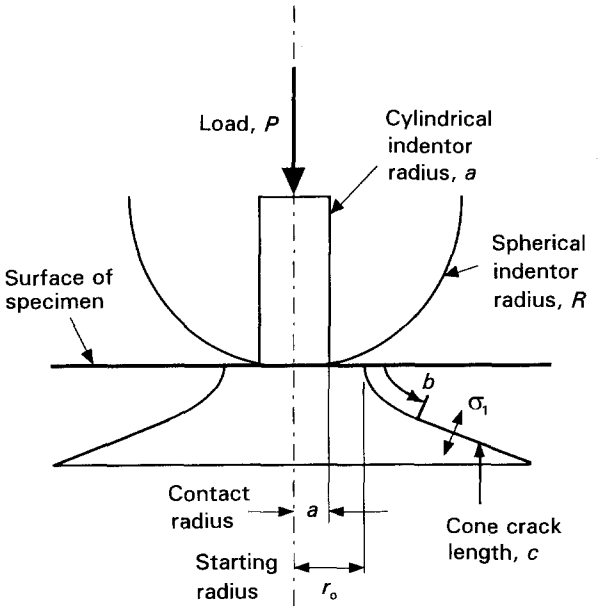


*Figure 2* Hertzian cone crack parameters.

where $A$ is termed the Auerbach constant. Equation 4 can be alternatively written in terms of the radius, $a$, of the contact region using Equation 1

$$P = \frac{4}{3}\left[\frac{AE}{k(1-\nu^2)}\right]^{1/2} a^{3/2} \quad (5)$$

Substituting Equation 4 into Equation 3 gives

$$\sigma_{max} = \left[\frac{(1-2\nu)A^{1/3}}{2\pi}\right]\left[\frac{4E}{3k(1-\nu^2)}\right]^{2/3} R^{-1/3} \quad (6)$$

If $\sigma_{max}$ is the maximum tensile stress upon the occurrence of a cone crack, then Auerbach's Law appears to imply that the tensile strength of the material depends on the radius of the indentor rather than being a material property – a size effect worthy of special note.

The classical Hertzian stress field assumes a condition of full slip between the indentor and the specimen. However, experiments described in the present work show that the inevitable presence of friction between the indentor and the specimen greatly influences the indentation stress field. Johnson *et al.* [9] have studied this phenomenon for spherical indentors. They found that the use of indentor and specimen materials of different elastic properties leads to frictional forces which effectively increase the fracture load when the indentor is more rigid than the specimen.

We have undertaken a finite element analysis of the indentation of a flat specimen with a rigid cylindrical indentor for both full slip and no slip contact. Fig. 1a–c show the stress fields for frictionless contact, whereas Fig. 1d shows the $\sigma_1$ radial stress along the specimen surface for conditions of both full slip and no slip. It can be seen from Fig. 1d that the radial tensile stress responsible for the formation of a classical Hertzian fracture all but disappears when the indentor is fully bonded to the specimen.

## 3. Fracture mechanics in the Hertzian stress field

In a classic work, Griffith [4] showed that the growth of a crack in a solid under stress can be described in terms of the energy needed to form new crack surfaces and the attendant release in strain energy. The externally applied uniform stress, $\sigma$, required for the growth of an existing flaw of length $2c$ and unit width is

$$\sigma \geqslant \left[\frac{2\gamma E}{(1-\nu^2)\pi c}\right]^{1/2} \quad (7)$$

where $\gamma$ is the fracture surface energy ($J\,m^{-2}$). The $1-\nu^2$ term is included for the general case of plane strain. Equation 7 applies directly to a double-ended crack of length $2c$ contained fully within a uniformly stressed solid. It may also be applied with only a small error to a half crack of length $c$, such as may be found on the surface of a solid [6, 10].

Irwin [10] showed that the Griffith criterion for fracture may be expressed in terms of a stress intensity factor, $K_I$, such that

$$\frac{K_I^2(1-\nu^2)}{E} \geqslant 2\gamma \quad (8)$$

where

$$K_I = \sigma(\pi c)^{1/2} \quad (9)$$

The left-hand side of Equation 8 is termed the strain energy release rate and is given the symbol $G$. The Griffith criterion is satisfied for $K_I \geqslant K_{IC}$. $K_{IC}$ can be considered to be a material property and is known as the plane strain fracture toughness.

$K_{IC}$ can be readily measured in the laboratory. A typical value for soda-lime glass is $0.78\ MPa\ m^{1/2}$. Using this value, Equation 8 gives a fracture surface energy, $\gamma = 3.6\ J\,m^{-2}$, which is in agreement with various experimentally determined values of this quantity [11].

Frank and Lawn [6] applied Irwin's concept of the stress intensity factor to the indentation stress field and showed how the progress of a crack can be described in terms of the prior stresses. If we consider an internal crack of length $2c$ within a solid loaded by an externally applied stress, $\sigma$, as shown in Fig. 3a, then the stress intensity factor, $K_I$, associated with the presence of the crack is readily determined from Equation 9. If a series of surface tractions, opposite in direction to the stress, is then applied to the crack faces so as to close the crack completely, as shown in Fig. 3b, then at this point, the stress distribution, uniform or otherwise, within the solid is precisely equal to that which would have existed in the absence of the crack. The stress intensity factor thus drops to zero because there is no longer a concentration of stress at the crack tip, the crack having been completely closed. The effect of the applied tractions in determining the stress intensity factors is therefore precisely equal (to within a sign) to that caused by the concentration of the macroscopic stress by the presence of the crack. The stress intensity factor can thus be determined from the pre-existing stress field in the solid.

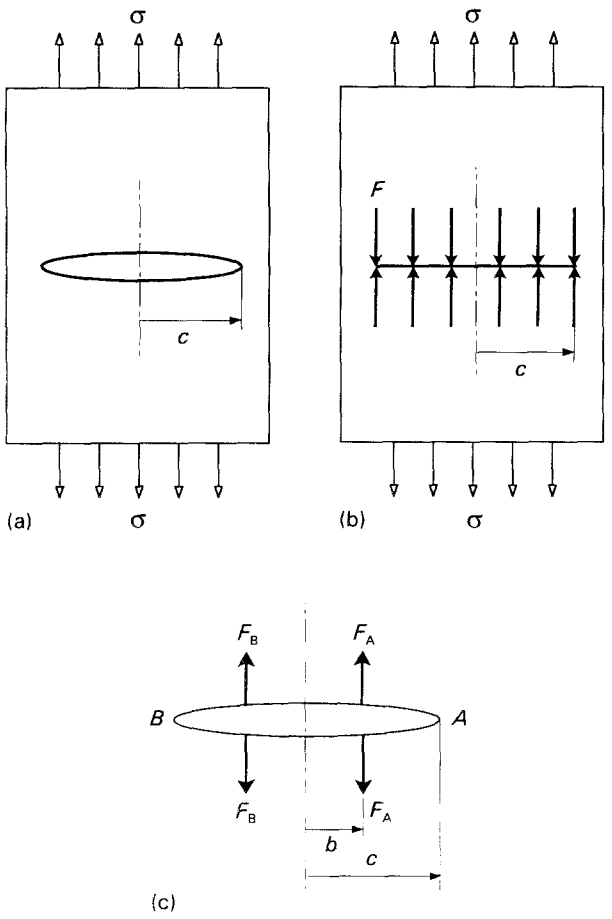


*Figure 3* (a) Internal crack in a solid loaded with an external stress, σ. (b) Crack closed by the application of a distribution of surface tractions $F$. (c) Internal crack loaded with surface tractions $F_A$ and $F_B$.

In order to calculate this stress intensity factor from the prior stress field, we may consider the situation illustrated in Fig. 3c. Irwin determined that the stress intensity factor, $K_I$, at one of the crack tips, A, for a symmetric internal crack being loaded by forces, $F_A$, applied on the crack faces to be

$$K_{IA} = \frac{F_A}{(\pi c)^{1/2}}\left[\frac{c+b}{c-b}\right]^{1/2} \quad (10)$$

As shown in Fig. 3c, forces $F_B$ also contribute to the stress field at A and Irwin calculated the stress intensity factor, due to those forces, to be

$$K_{IB} = \frac{F_B}{(\pi c)^{1/2}}\left[\frac{c-b}{c+b}\right]^{1/2} \quad (11)$$

An important property of stress intensity factors is that they are additive for the same type of loading. Therefore, the total stress intensity factor at crack tip A shown in Fig. 3c due to forces $F_A$ and $F_B$, for symmetric loading, where $F_A = F_B = F$, is

$$K_I = K_{IA} + K_{IB} = \frac{2F}{\pi^{1/2}}\left[\frac{c}{(c^2-b^2)}\right]^{1/2} \quad (12)$$

Now, if, as we have stated previously, the Griffith energy balance criterion, as given by Equation 7, applies to both a single-ended and double-ended crack, then we may equally well say that Equation 12 gives a good approximation to the stress intensity factor for a single-ended crack of length $c$. Both assumptions rely on the approximation that the stress field in the vicinity of the crack tip is little affected by forces or stresses at the opposite end of an equivalent double-ended crack.

If the tractions are continuous along the length of the crack, but are directed so as to close the crack completely, then the force per unit length may be associated with a stress, σ, where $F = \sigma(b)db$. The total stress intensity factor is given by the integral

$$K_I = \frac{2}{\pi}\int_0^c c^{1/2}\frac{\sigma(b)}{(c^2-b^2)^{1/2}}db \quad (13)$$

where $c$ is the length of the crack and $\sigma(b)$ is then the prior stress distribution within the solid along the crack path. The stress intensity factor, as calculated by Equation 13 for surface tractions applied so as to close the crack, is precisely the same as that calculated for the crack in the absence of such tractions, which, for the uniform stress case, is given by Equation 9. Thus, the energetics associated with the growth of a crack within any stress field may be completely described by the prior stresses using Equation 13.

Early workers applied the Griffith fracture criterion to flaws in the vicinity of an indentor in terms of the surface tensile stress only, as given by the Hertz equations. Combining Equations 3 and 7 gives the critical condition for failure as

$$\left[\frac{2E\gamma}{(1-\nu^2)\pi c}\right]^{1/2} = \left[\frac{(1-2\nu)}{2\pi}\right]\left[\frac{4E}{3(1-\nu^2)k}\right]^{2/3}\frac{P^{1/3}}{R^{2/3}} \quad (14)$$

Equation 14 states that $P$ is proportional to $R^2c^{-3/2}$. If all the flaws in a specimen were of a uniform size, then the Griffith energy balance criterion would appear to predict that $P$ is proportional to $R^2$, in contradiction to Auerbach's empirical law.

Some workers [5, 12] have attempted to explain Auerbach's law in terms of the surface flaw statistics of the specimen. It was argued that for a larger indentor radius, the increased chance that the region of maximum tensile stress would include a particularly large flaw may result in the formation of a cone crack at a reduced load, thus reducing the $R^2$ dependency.

The main criticisms of the flaw statistical explanation are:

(a) it is extremely improbable that every piece of material would have the exact flaw distribution required to produce the linear form of Auerbach's law;

(b) because smaller indentors sample smaller areas of specimen surface, the scatter in results would be expected to increase with decreasing $R$. Langitan and Lawn [13] claim that this is not observed, although the data of Hamilton and Rawson [5] appear to show otherwise;

(c) the flaw statistical explanation predicts that if all flaws were of the same size, then $P$ is proportional to $R^2$ if one applies the Griffith energy balance criterion as given by Equation 14. Langitan and Lawn [13]

show that there does exist a range of flaw sizes for which Auerbach's law still holds even when all flaws are of the same size.

The apparent violation of the Griffith energy balance criterion shown by the previous analysis is a consequence of the assumption that the stress distribution along the length of a cone crack is uniform, and equal to the surface stresses given by the Hertz equations. In a more rigorous application of the Griffith criterion, Frank and Lawn [6] included the effect of the changing level of stress along a crack path which started at the radius of the circle of contact and followed the $\sigma_3$ stress trajectory. Their analysis showed that Auerbach's law was a consequence of the formation of a hitherto unobserved shallow ring crack which preceded the formation of the more familiar cone crack. In an important development, Mouginot and Maugis [7] investigated the effect of the starting radius on the Griffith energy balance criterion applied in this manner. They noted that Frank and Lawn's theory unfortunately neglected the effect of the starting radius, which is always larger than that of the contact circle, and that they also used an artificially high value of Poisson's ratio in their calculations. The work of Mouginot and Maugis shows that Auerbach's law is a consequence of the peculiar nature of the diminishing stress field which, together with the radius of the indentor, influences the starting radius of the cone crack and hence its subsequent progress through the bulk of the specimen. They argued that for a high density of flaws of uniform size, the cone crack is initiated at the radius for which the strain energy release rate is greatest. In certain cases, the existence of a seminal ring crack is predicted, but this feature was shown to be of less significance than the work of Frank and Lawn suggests. We now summarize the essential features of the analysis of Mouginot and Maugis.

In indentation work, it is usual to normalize the units for stress in terms of the mean pressure, $p_m$, under the indentor, and the units of distance in terms of the radius of the circle of contact, $a$. Hence, we may define

$$f(b/a) = \frac{\sigma(b/a)}{p_m} \tag{15}$$

where

$$p_m = \frac{P}{\pi a^2} \tag{16}$$

To account for the change in stress intensity factor for a developing cone crack in which the width of the crack front increases as the crack path increases, Mouginot and Maugis include a correction in Equation 13 to give

$$K_I = \frac{2}{\pi}\int_0^c c^{1/2}\frac{r_b}{r_c}\frac{\sigma(b)}{(c^2 - b^2)^{1/2}}\mathrm{d}b \tag{17}$$

where $2\pi r_c$ represents the length of the crack front at the tip of the cone crack, and $2\pi r_b$ is the crack length at the point defined by the variable $b$ at which $\sigma(b)$ applies. In this form, the integral includes the change in length of crack front as $b$ increases from 0 to $c$.

A function $\phi(c/a)$ may be written as

$$\phi(c/a) = \frac{c}{a}\left[\int_0^c \frac{r_b}{r_c}\int f(b/a)\Big/\left(\frac{c^2}{a^2} - \frac{b^2}{a^2}\right)^{1/2}\right]\mathrm{d}\left(\frac{b}{a}\right)\Bigg]^2 \tag{18}$$

where $f(b/a)$ is given by Equation 15. Equation 18 allows the Griffith criterion at the critical fracture condition to be expressed as

$$G = 2\gamma = \frac{4(1 - \nu^2)P^2}{\pi^3 E a^3}\phi(c/a) \tag{19}$$

The function $\phi(c/a)$ contains an integral which is characteristic of the pre-existing stress field. The function $\phi(c/a)$ must be evaluated for a particular starting radius, $r_0/a$, because this determines the values of the stress along the crack path.

$\phi(c/a)$ can be determined from the stress field for either spherical or flat punch indentors as calculated by Sneddon [14], and Barquins and Maugis [15]. The integral may then be calculated numerically and the strain energy release rate determined for small increments of crack length.

Rearranging Equation 19 gives the critical load for fracture as

$$P_c = \left[\frac{a^3}{\phi(c/a)}\right]^{1/2}\left[\frac{\pi^3 E 2\gamma}{4(1 - \nu^2)}\right]^{1/2} \tag{20}$$

The factors in the second term on the right-hand side of Equation 20 are all material constants. It would appear, therefore, that Auerbach's empirical law would be consistent with the analysis if $\phi(c/a)^{1/2}$ is also a constant, because then the critical load would be proportional to $a^{3/2}$, (which according to Equation 5, is equivalent to Auerbach's law). However, $\phi(c/a)^{1/2}$ cannot be assumed constant because it contains terms for the stress field, the initial flaw size and indentor radius, all of which are variables. It is later shown that there is a range of values of stress level, indentor radius and flaw sizes for which $\phi(c/a)^{1/2}$ is nearly constant. This range of $c_f/a$ is, therefore, called the "Auerbach range".

Fig. 4 shows values for $\sigma_1$ along the path of the $\sigma_3$ stress trajectory for different starting radii. These results were obtained from a numerical analysis using the finite-element method for the case of a rigid, cylindrical indentor with a condition of full slip between the indentor and the specimen. The dotted line shows an analytical result obtained by Mouginot and Maugis for one value of $r_0/a$.

For a surface with a high density of flaws, the largest strain energy release rate for a given flaw size determines where and at what load a flaw will develop into a crack. Values of $\phi(c/a)$ for cracks at different starting radii $r_0/a$ are shown in Fig. 5. The value of $\phi(c/a)$ for any particular normalized radius $r_0/a$ is proportional to the strain energy release rate for a crack of size $c/a$ which commences at that radius $r_0/a$. For any flaw size $c_f$, there is a particular radius, $r_0$, for which the strain energy release rate is greatest. This corresponds to the upper envelope of the curves of $\phi(c/a)$ in Fig. 5. We denote this upper envelope as $\phi(c_f/a)$. When the

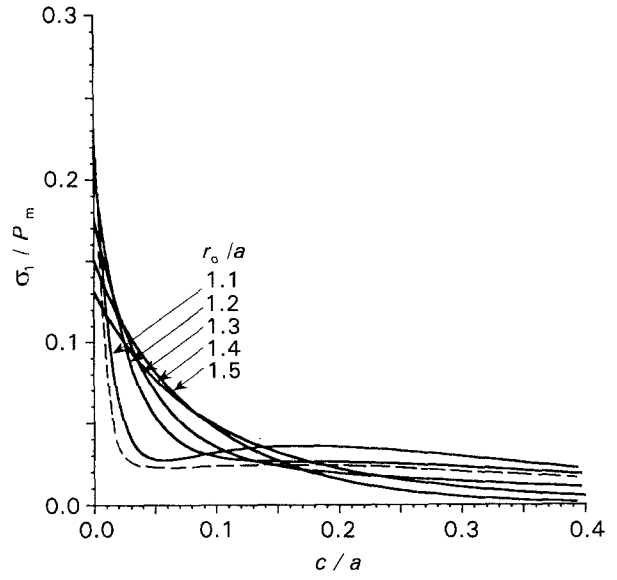


*Figure 4* Normalized radial stress $\sigma_1/P_m$ plotted as a function of normalized distance $c/a$ along the $\sigma_3$ stress trajectory for different starting radii, $r_0/a$ (cylindrical flat punch indentor, full slip). (. . .) The analytical result of Mouginot and Maugis [7] for $r_0/a = 1.1$.

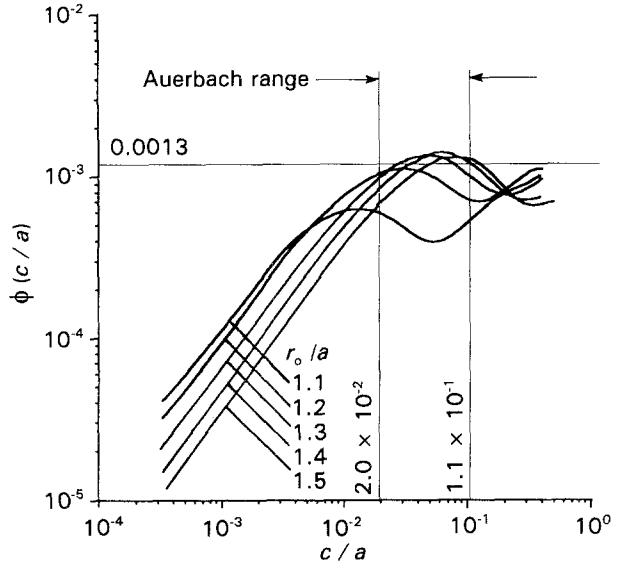


*Figure 5* Strain energy release function $\phi(c/a)$ as a function of normalized crack length, $c/a$, for different starting radii, $r_0/a$ (cylindrical, flat punch indentor, full slip). The Auerbach range where the outer envelope of $\phi(c/a)$ is approximately constant, is indicated.

indentor load is steadily increased, the Griffith criterion will be first met when the strain energy release rate, as defined by the upper envelope in Fig. 5, becomes equal to twice the fracture surface energy. A cone crack will initiate at the lowest load for which a flaw of size $c_f/a$ exists in the specimen at a radius for which $\phi(c_f/a)$ is greater than the critical value.

For a high density of very small flaws, in the size range $c_f/a < 0.01$, the critical load $P_c$, given by Equation 20, decreases as the flaw size increases because the stress level along the length of the flaw is fairly constant and is approximately equal to the surface stress as given by the Hertz equation. In this case, the Griffith criterion for a uniform constant stress level may be employed. Smaller flaws are more likely to extend at a lower $r_0/a$ because the surface stress level is higher closer to the contact radius. Auerbach's law would not hold in this case.

For larger flaws, in the size range $0.1 < c_f/a < 0.2$, the situation is qualitatively different. Equation 20 and Fig. 5 show that the critical load increases with increasing flaw size because the strain energy release rate given by $\phi(c/a)$ decreases with increasing flaw size. The reason for this surprising result is in the form of the integral in Equation 18. The strain energy release rate depends on both the stress distribution along the flaw and the factor $(c^2 - b^2)^{-1/2}$. Larger values of $c$ cause the integral to evaluate to a lower value compared to smaller flaws at the same $r_0$.

From Equation 20, $P_c/a^{3/2}$ is proportional to $\phi(c_f/a)^{-1/2}$. Fig. 5 shows that there is a range of $c_f/a$ where the outer envelope, $\phi(c_f/a)$, is fairly constant. This is the Auerbach range. In this range, the critical load $P_c$ which initiates fracture is nearly independent of the flaw size and is therefore proportional to $a^{3/2}$. If we assume the existence of flaws of all sizes everywhere on the specimen surface, then for a particular flaw size, the starting radius is that which gives the maximum strain energy release rate. The Griffith criterion will be first met, upon an increasing load, at the position where the maximum strain energy release rate occurs. For another flaw size, the starting radius is different but the strain energy release rate, and hence the critical load, is not much different.

For flaws within the Auerbach range of flaw sizes, the minimum critical load is given the symbol $P_a$ and is found from

$$P_a = \left[\frac{E\pi^3\gamma a^3}{(1 - \nu^2)2\phi_a}\right]^{1/2} \tag{21}$$

where $\phi_a$ is the value of $\phi(c/a)$ at the plateau. From Fig. 5, we estimate this to be at $\phi(c/a) = 0.0013$. Mouginot and Maugis estimate $\phi(c/a) = 0.001$ from their analytically derived stress field. The value of $\phi_a$ is important because it influences the fracture surface energy which is estimated from data obtained from experiments. It should be noted that the curves in Fig. 5 apply to a cylindrical indentor. Mouginot and Maugis show that a similar set of curves can be generated using the stress field associated with a spherical indentor, which results in a slightly different value of $\phi_a$. In this work, we are concerned primarily with cylindrical indentors.

It is clear from the above discussion that the application of the Griffith energy balance criterion for fracture relies on a precise knowledge of the indentation stress field. Classical analytical results [14, 15] assume frictionless contact between the indentor and the specimen. Our finite-element work demonstrates a marked reduction in the magnitude of the radial tensile stress in the vicinity of the indentor in the presence of interfacial friction. Thus, it is reasonable to expect that for a contact involving friction, larger indentor loads would be required to raise the tensile stress to a level capable of inducing the formation of a cone crack. Our experimental results, to be presented

below, indicate that friction cannot be totally eliminated. Although we recognize the difficulty of including frictional forces in the above analytical treatment precisely, as a first approximation, we propose the inclusion of an additional factor, $\beta$, in Equation 21 which has the effect of raising the indentor load required to satisfy the Griffith criterion. The inclusion of the factor $\beta$ is purely empirical and we later show that although there is no theoretical reason to expect that frictional forces can be accommodated by such a simple adjustment, reasonable agreement between theory and experiment can nevertheless be obtained. Equation 22 shows our proposed expression for the minimum fracture load

$$P_a = \left[\frac{E\pi^3\beta\gamma a^3}{(1-\nu^2)2\phi_a}\right]^{1/2} \quad (22)$$

We define "fracture" to signify the event when a flaw extends immediately to form a circular ring crack concentric with the contact radius. Once a flaw has become a propagating crack, it extends according to the strain energy release function curve, Fig. 5, appropriate to its starting radius. The development of this starting flaw into a ring crack precludes the extension of other flaws in the vicinity, even though the value of $\phi(c/a)$ for those flaws at some applied load above the flaw initiation load may be larger than that calculated for the starting flaw as it follows its $\phi(c/a)$ curve. This is because the conditions which determine crack growth depend on the prior stress field. The function $\phi(c/a)$ can be used to describe the initiation of crack growth for all flaws which exist in the prior stress field but can only be considered applicable for the subsequent elongation for that flaw which actually first extends.

In the next section, we show how the strain energy release rate argument developed by Mouginot and Maugis can be used to determine a probabilistic criterion for fracture for a given indentor load, radius and surface-flaw distribution.

## 4. The probability of Hertzian fracture

It is well known that both the size and distribution of surface flaws characterize the strength of brittle solids. The experimentally observed strength of glass can be conveniently described by Weibull statistics. In general terms, the probability of failure of a sample of glass of area $A$, subject to a uniform tensile stress $\sigma$, can be expressed empirically by [8]

$$p_f = 1 - \exp(kA\sigma^m) \quad (23)$$

where $m$ and $k$ are called the Weibull parameters, which can only be determined by experiment. The parameter $m$ describes the spread in strengths (a large value indicating a narrow range) and the parameter $k$ is associated with the "reference strength" and the surface-flaw density of the specimen. The Weibull parameters can be considered as material constants to the extent that once determined for a known stress distribution, the probability of failure can be calculated for a similar surface with a different stress distribution.

The probability of failure given by Equation 23 is precisely equal to the probability of finding a flaw within an area $A$ of the specimen which is larger than the critical flaw size (as given by the Griffith criterion) for a uniform stress, $\sigma$. The critical flaw size is given by Equation 9.

Brown [16] determined Weibull parameters for as-received soda–lime glass sheets subjected to a lateral uniform pressure and found $m = 7.3$ and $k = 5.1 \times 10^{-57}\ m^{-2}\ Pa^{-7.3}$. Beason [17] used results of tests on 20 year old weathered glass to derive values of $m = 6$ and $k = 7.19 \times 10^{-45}\ m^{-2}\ Pa^{-6}$. For 1 $m^2$ area samples, it can be shown that these results correspond to a probability of failure of 50% for an applied uniform tensile stresses of 48 MPa for as-received glass, and 21 MPa for weathered glass. Corresponding flaw sizes are 0.3 and 1.1 mm, respectively. Because the actual tests were done with a uniform pressure, the flaw sizes which actually cause fracture will probably be larger than these values because the surface stress distribution is non-uniform throughout the thickness of the sample.

This flaw size range is significant because it may influence the accuracy with which we can apply these Weibull parameters to indentation tests which by their nature sample only very small areas and hence very small flaws.

Turning now to Hertzian fracture, in general there may exist a considerable number of flaws of lengths below, above and within the Auerbach range on the surface of a specimen. The probability of failure for a given indentor load depends directly upon the probability of finding a surface flaw capable of causing fracture under the prevailing stresses near the surface within the area of solid around the indentor which is subjected to tensile stress. Critical stress and flaw size are related by Equation 9 when the stress is applied along the full depth of the flaw. In an indentation stress field, however, this only applies for very small flaws where the tensile stress is given by Hertz's equations. The uniform stress field approximation becomes progressively worse as the Auerbach range is approached.

For larger flaws, within the Auerbach range, the fracture load becomes nearly independent of the flaw size because the maximum strain energy release rate, as described by the outer envelope of the curves of Fig. 5, is approximately constant. The probability of fracture from these flaws must, therefore, be expressed in terms of the probability of finding a flaw of the required size at a starting radius commensurate with the curves of Fig. 5. We now describe a method whereby this may be achieved.

Consider a specimen supporting a cylindrical indentor of radius $a$ with load $P$. Let $P_a$ be the minimum critical load for values of $c/a$ within the Auerbach range. As noted above, the value of the function $\phi(c/a)$ can be estimated for flaw sizes within the Auerbach range by inspection of Fig. 5. We estimate this to be at $\phi_a = 0.0013$. Fig. 6 shows the relationship between the normalized strain energy release rate $G/2\gamma$, flaw size $c/a$, and starting radius $r_0/a$, for three different values of $P$: $P_{a-}$, a load below the minimum critical load; $P_a$,

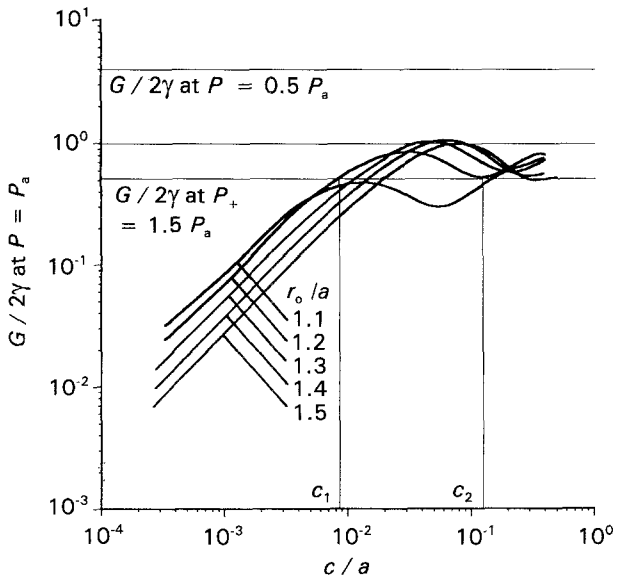


*Figure 6* Relationship between strain energy release rate, $G$, and flaw size, $c/a$, for different indentor loads, $P/P_a$. The vertical axis scaling applies to $P/P_a = 1$. The vertical axis positions for the condition $G = 2\gamma$ for different ratios $P/P_a$ are drawn relative to the family of curves shown. The flaw size range for $G/2\gamma > 1$ for a starting radius $r_0/a = 1.2$ for $P/P_a = 1.5$ is indicated.

the minimum critical load; and $P_{a+}$, a load greater than the minimum critical load. The Griffith criterion is met when $G/2\gamma \geqslant 1$. On this diagram, the line $G/2\gamma = 1$ has been drawn at positions corresponding to $P_{a-}$, $P_a$ and $P_{a+}$. This allows the graph to be presented more clearly, showing only one family of curves. The curves shown in Fig. 6 rely only upon the choice of $\phi_a$ and are independent of the value of $\gamma$. However, if one wishes to draw curves as in Fig. 6 for a particular indentor load, then $P_a$ must be first determined from Equation 21, which requires an estimate of $\gamma$, or from Equation 22 in the more general case with friction, which requires an estimate of both $\gamma$ and $\beta$.

It is immediately evident that if the load is less than the minimum critical load $P_a$, failure will not occur from any flaws, no matter how large, because the Griffith criterion is never met. It can be seen that failure can only occur from flaws within the Auerbach range for loads equal to or greater than $P_a$. Fracture from flaws of size below, including, and beyond the Auerbach range can only occur if the load is greater than $P_a$.

At a load $P_{a+}$, greater than $P_a$, the Griffith criterion is met for various ranges of flaw sizes which depend on the particular values of starting radii. Fracture will occur from a flaw located at a particular starting radius if that flaw is within the range for which $G/2\gamma \geqslant 1$ for that radius. This range of flaw sizes can be determined from Fig. 6 and is given by the $c/a$ axis coordinates for the upper and lower bounds of the region where $G/2y > 1$ for the curve which corresponds to the radius under consideration. We have therefore reduced the problem of calculating the probability of indentation fracture occurring at a particular radius and load to the probability of finding at least one flaw within a specific size range at that radius.

To determine these probabilities, it is convenient to divide the area surrounding the indentor into $n$ annular regions of radii $r_i$ ($i = 1$–$n$). To determine the probability of finding a flaw which meets the Griffith criterion within each annular region, Equation 23 may be used. Equation 23 gives the probability of failure for an applied uniform stress, but also can be used to calculate the probability of finding a flaw of size greater than or equal to the critical value for that stress, as given by Equation 9, within an area $A$ of the surface of the solid. The strength parameters, $m$ and $k$, for Equation 23 are those which are appropriate to the specimen surface condition.

The probabilities calculated for each annular region can be suitably combined to yield a total probability of failure for a particular indentor load and radius for a given surface flaw distribution.

We proceed as follows. Curves as shown in Fig. 6 are drawn for a particular value of indentor load $P$. Consider one of the annular regions with radius $r_i$ and area $\delta A_i$. The range of values of flaw size which satisfies the Griffith criterion may be determined for this region by considering the appropriate line for $\phi(c/a)$ in Fig. 6. For example, the vertical lines in Fig. 6 show the range of flaw sizes, for $P/P_a = 1.5$, which, should they exist within the increment centred on $r_i/a = 1.2$, will cause fracture at that radius. Let this range be denoted by $c_1 \leqslant c \leqslant c_2$. We therefore require the probability of finding such a flaw within this size range in the area $\delta A_i$. This is equal to the difference between the probability of finding a flaw of size $c > c_1$ and the probability of finding a flaw of size $c > c_2$. However, the probability of finding a flaw of size greater than a specific size, say $c_1$, within the area $\delta A$ is precisely equal to the Weibull probability of failure (Equation 23) under the corresponding critical stress as given by Equation 9.

Once a particular indentor size has been specified, then the probability of finding a flaw of size greater than $c_1$ within the annular region of radius $r_i$ and width $\delta r_i$, which has an area $\delta A_i = 2\pi r_i \delta r_i$, is

$$p_i(c > c_1) = 1 - \exp\left\{ - k2\pi r_i \delta r_i \left[ \frac{K_{IC}}{(\pi c_1)^{1/2}} \right]^m \right\} \quad (24)$$

Similarly, the probability of finding a flaw of size greater than $c_2$ within the same area element $\delta A_i$ is given by

$$p_i(c > c_2) = 1 - \exp\left\{ - k2\pi r_i \delta r_i \left[ \frac{K_{IC}}{(\pi c_2)^{1/2}} \right]^m \right\} \quad (25)$$

The probability of finding a flaw of size in the range $c_1 \leqslant c \leqslant c_2$ within area $\delta A_i$ is the difference in probabilities given by Equations 23 and 24 and is equal to the probability of failure from a flaw of size within that range

$$p_{f_i}(c_1 \leqslant c \leqslant c_2) = p_i(c > c_1) - p_i(c > c_2) \quad (26)$$

The values $c_1$ and $c_2$ may be determined for all annular regions by inspection of Fig. 6. Because a two-parameter Weibull function gives a non-zero probability of failure for even the lowest stresses, it would appear that the upper limit of $r_i/a$ should extend to the full dimensions of the specimen where the effect of the indentation stress field may still be apparent. However, if one is interested in loads near to the minimum

critical load for flaws within the Auerbach range, $P_a$, then it is necessary to consider only starting radii which correspond to the upper end of the Auerbach range, that is, $r_i/a = 1.5$ which gives a maximum $\phi(c_f/a)$ at $c/a = 0.1$.

The probability of fracture not occurring from a flaw within the region $\delta A_i$ is found from

$$p_{s_i} = 1 - p_{f_i} \quad (27)$$

The probability of survival for the entire region of $n$ annular elements surrounding the indentor is thus given by

$$p_s = p_{s_1} p_{s_2} p_{s_3} p_{s_i} \cdots p_{s_n} \quad (28)$$

Therefore, finally, the probability of failure, $p_f$, for the entire region, at the load $p/p_a$, is then given by:

$$p_F = 1 - p_S \quad (29)$$

This calculation is repeated for different values of $p/p_a$ to obtain values of probability of failures for a particular value of indentor radius, $a$.

Probabilities of failure for both as-received and weathered glass have been calculated for a range of cylindrical indentor sizes corresponding to those used in indentation experiments by various workers. The results for as-received and weathered glass are shown in Figs 7 and 8, respectively, where the fracture load has been expressed as a force rather than the ratio $P/P_a$.

The curves in Figs 7 and 8 rely on an estimation of the fracture surface energy, $\gamma$ (and also the factor $\beta$, if interfacial friction is to be included) in Equations 21 and 22. Although the fracture surface energy may, in principle, be determined from indentation tests, we believe that such estimations are inaccurate due to the inevitable presence of friction between the indentor and the specimen. For example, if friction is assumed to be negligible, the fracture data reported by Langitan and Lawn [13], and our own data, to be

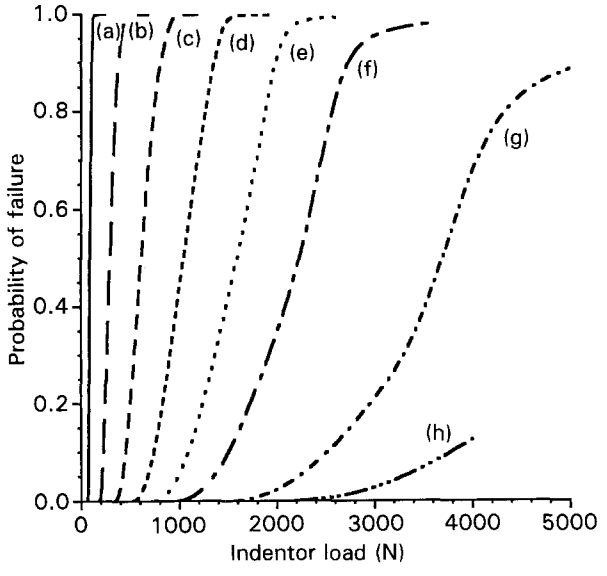


*Figure 7* Calculated probability of failure versus indentor load for a range of cylindrical indentor radii for as-received glass. Indentor radii (mm): (a) 0.1, (b) 0.2, (c) 0.3, (d) 0.4, (e) 0.5, (f) 0.6, (g) 0.8, (h) 1.0.

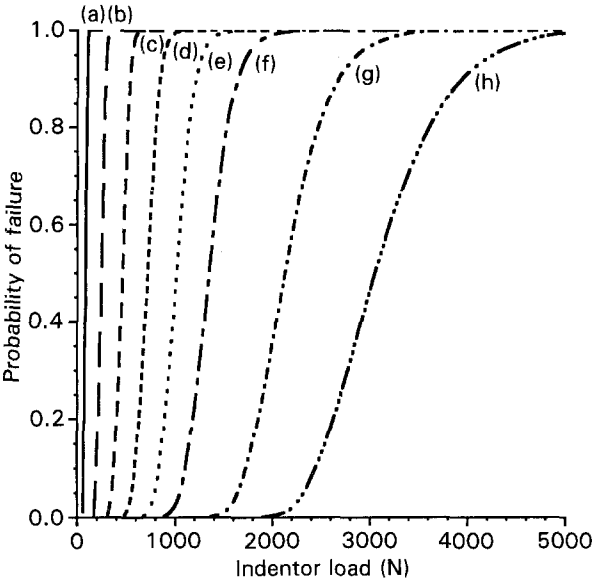


*Figure 8* Calculated probability of failure versus indentor load for a range of cylindrical indentor radii for weathered glass. (a–h) See Fig. 7.

presented shortly, imply a fracture surface energy in the order of $10\,J\,m^{-2}$ which seems to be too large. However, for the purposes of calculating data for Figs 7 and 8, we have assumed frictionless contact, $\beta = 0$, and a fracture surface energy $\gamma = 3.6\,J\,m^{-2}$ calculated from Equation 8 and $K_{IC} = 0.78\,MPa\,m^{1/2}$. The effect of friction could be included in the data of Figs 7 and 8 by re-scaling the values of indentor load by a factor $\beta^{1/2}$.

In Figs 7 and 8, the cut-off at $P_a$ for each indentor size indicates a zero probability of failure for loads below the minimum critical load. Figs 7 and 8 also show that, as expected, the spread in fracture loads is less for weathered glass than for as-received glass. However, the minimum critical load remains the same.

It is of interest to note that we have expressed the probability of indentation failure in terms of Weibull statistics which were determined from bending tests involving a stress field which is nearly constant with depth over a distance characteristic of the flaw size. This is possible because we are expressing the probability of indentation failure in terms of the probability that certain areas of surface contain flaws within various size ranges. This probability is a property of the surface and the surface strength parameters $m$ and $k$ may be determined through bending tests. A suitable combination of these probabilities gives the probability of failure for the special case of the diminishing stress field associated with an indentation fracture.

## 5. Hertzian fracture data

Many indentation experiments described in the literature have used spherical indentors. The present work includes experiments with both cylindrical and spherical indentors although our theoretical analysis focuses exclusively on cylindrical indentors. In this section we compare previously published Hertzian

fracture data with our own experimental results and theoretical predictions.

### 5.1. Experimental procedure

Indentations were made with hardened steel cylindrical punches on both as-received and abraded specimens of soda–lime glass. Tests were also carried out using hardened steel spherical indentors. For both cylindrical and spherical indentors, the effects of lubricated and non-lubricated contacts were investigated.

The cylindrical punch indentors were machined from silver steel and subsequently hardened by heat treatment. The ends of the punches were ground and polished. The spherical indentors were commercially available steel ball bearings. The glass specimens were as-received soda–lime float glass sheets measuring 220 mm × 140 mm × 4 mm, all cut from the same parent plate. No special cleaning or surface preparation was carried out prior to testing. For the tests involving abraded specimens, the glass sheets were abraded in perpendicular directions on one side only using wet-and-dry 320 grit abrasive paper. It is interesting to note that various methods of abrasion have been used in previous work of this kind. For example, Mouginot and Maugis [7] used mainly abrasive paper, whereas Langitan and Lawn [13] used a slurry of silicon carbide grit.

For those tests involving lubricated contact between indentor and the specimen, the indentor was dipped into machine cutting fluid (a high-pressure lubricant) prior to each indentation.

The glass sheets were placed on the bed on an Instron 4302 testing machine fitted with a 10 kN load cell. Each indentor was forced onto the specimen surface with a crosshead speed of 0.5 mm $min^{-1}$. The indentor load was noted at the instant a cone crack became visible through a microscope positioned for this purpose. About 20 indentations were made for each punch diameter.

For non-lubricated cylindrical indentors on as-received glass, it was observed that plastic deformation of the punch occurred due to the large loads required to initiate fracture. The deformation resulted in a permanent increase in the punch diameter of about 25% although the ends remained very nearly flat. Further testing revealed no additional increase in diameter. The enlarged punch diameter, after deformation, is used in the presentation of the results for this specimen surface condition.

A series of indentations was carried out on both sides of one particular as-received specimen to establish whether or not the glass had suffered different levels of abrasion during manufacture and handling. Hamilton and Rawson [5] obtained significantly lower mean fracture loads for the tin bath side of their float glass and inferred that this side was damaged as the glass sheet passed over various rollers during manufacture. In our experiments, however, the results from both sides were indistinguishable.

It was observed that for cylindrical indentors with dry contact on as-received glass, conical indentation fracture did not occur. Instead, the specimen fractured catastrophically. However, normal Hertzian cone cracks were obtained with lubricated contact between the indentor and the specimen.

The conical cracks obtained in the experiments of the present work were typical Hertzian cone cracks as reported in the literature. An inner ring on the surface of the specimen marked the indentor contact area and a larger ring, slightly eccentric to the inner ring, indicated the beginning of the cone crack. The point of initiation of the crack was readily apparent and an area containing radial striations indicated the region where the crack was both travelling downwards and around the contact area. The location of the meeting of the two ends of the crack as they travelled around the contact area was diametrically opposite to the starting location. Well-formed cones were observed for both cylindrical and spherical indentors.

### 5.2. Characteristics of Hertzian fracture

Two parameters derived from indentation fracture data may be considered for comparison purposes: the minimum critical load for failure and the mean or median load for failure. For abraded specimens, we expect there to be little difference between the minimum and mean fracture loads. Following Hamilton and Rawson [5], we make no distinction between the mean load and the median fracture load, although it should be noted that the median fracture load corresponds to a probability of failure of precisely 50%.

#### *5.2.1. Minimum critical fracture load*

As before, we let $P_a$ denote the minimum critical load for an indentation fracture to occur. We would expect this minimum critical load to correspond to the fracture load observed in experiments on glass with a high density of flaws, that is, on abraded glass. All experiments involve some degree of experimental error and our own experience indicates that there will always be some variation in fracture loads, even for well-abraded specimens. Thus, although in this section we are concerned with the minimum load for failure, we assume that this is represented by the mean load when reporting results from tests on abraded specimens. In making this assumption, we are implying that the degree of abrasion is sufficient to introduce flaws of a size within the Auerbach range uniformly throughout the surface of the specimen and that variations actually observed arise from experimental causes only. Experiments with abraded specimens [13] typically show only a standard deviation of about 5% compared to 20%–30% for as-received specimens.

Fig. 9a shows the minimum critical load, as determined from the mean fracture load for abraded glass specimens, reported in various literature sources [7, 13] for spherical indentors. Also shown in Fig. 9a are the experimental results of the present work for spherical indentors on abraded glass for both lubricated and non-lubricated contact.

Equations 21 and 22, in combination with Equation 1, predict a straight line relationship between spherical indentor radius and minimum critical load.

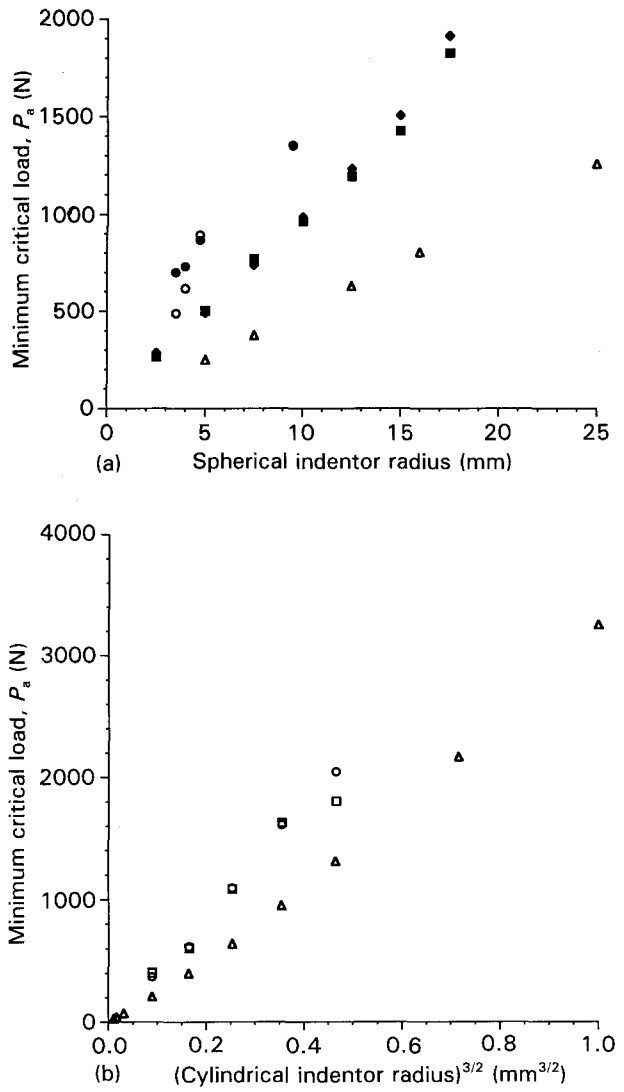


*Figure 9* Minimum critical fracture load versus indentor radius for abraded glass from various literature sources and the experimental data of the present work: (a) Spherical indentors, (b) cylindrical indentors. (a) (●) Experiment, abraded 320, lubricated soda–lime float; (○) experiment, abraded 320, non-lubricated soda–lime float; (◆) [13], abraded 600, soda–lime plate; (■) [13], abraded 400, soda–lime plate; (△) [7], abraded 400, borosilicate. (b) (□) Experiment, abraded 320, non-lubricated soda–lime float; (○) experiment, abraded 320, lubricated soda–lime float; (△) [7], abraded 400, borosilicate.

This is expected because Equation 21 assumes a specimen surface containing flaws of all sizes and does not give any information about the probability of finding a particular sized flaw at a particular starting radius. As the indentor size is increased, the flaw size corresponding to the Auerbach range also increases and it is from flaws within the Auerbach range that failure first occurs, because the function $\phi(c/a)$, as shown in Fig. 5, is a maximum in the Auerbach range of flaw sizes. Even though our theoretical work is concerned primarily with cylindrical indentors, the theory leading to Equations 21 and 22 is just as applicable to spherical indentors, the contact area, $a$, being related to the indentor radius, $R$, by Equation 1, and where the function $\phi(c/a)$ applies to the corresponding stress field for a spherical indentor.

The experimental data of the present work for spherical indentors does not agree particularly well with those of the 1969 results of Langitan and Lawn who used abraded "plate" glass. Both our results and those of Langitan and Lawn significantly different from those of Mouginot and Maugis, who used abraded borosilicate glass. According to Equations 21 and 1a, the slope of the linear regions of the data of Fig. 9a is directly proportional to the fracture surface energy, $\gamma$. In this work, we cannot apply Equation 21 directly to the data in Fig. 9a, for spherical indentors, because our estimate of $\phi_a = 0.0013$ was made using the stress field associated with a cylindrical indentor. However, the general form of Equation 21 still applies, and it is evident from the slope of the data in Fig. 9a that the fracture surface energy estimated by Mouginot and Maugis is some two to three times lower than that which would be determined from both our data and that of Langitan and Lawn. It should be noted that Mouginot and Maugis [7] estimate a fracture surface energy of $4.5\,J\,m^{-2}$ from their data, which is in good agreement to a predicted value of $5.2\,J\,m^{-2}$ for borosilicate glass for $K_{IC} = 0.85\,MPa\,m^{1/2}$. Fig. 9a also shows that there appears to be little difference in the fracture loads for lubricated and non-lubricated contact for spherical indentors on abraded specimens.

Fig. 9b shows the mean fracture loads for cylindrical indentors on abraded glass from both the present work and data estimated from Fig. 21 of Mouginot and Maugis [7]. As before, for abraded specimens, we assume that the mean load corresponds to the minimum critical load, $P_a$. Note that Fig. 9b shows data for fracture load as a function of $a^{3/2}$ which, if Auerbach's law holds as in Equation 21, should give a linear relationship with $P_a$. It is evident that if Equation 21 truly describes the indentation process, then the fracture surface energies implied in the present work are considerably higher than the $3.6\,J\,m^{-2}$ previously calculated for soda–lime glass. Mouginot and Maugis determined a fracture surface energy of $4.2\,J\,m^{-2}$ from their data for cylindrical indentors with $\phi_a = 0.001$. The fracture surface energy implied by the results of the present work, for a non-lubricated indentor, is considerably higher. From Equation 21, we calculate a fracture energy of $17\,J\,m^{-2}$ with $\phi(c/a) = 0.0013$, or $13.3\,J\,m^{-2}$ with $\phi_a = 0.001$. The slope of the data in Fig. 9b is proportional to the square root of the fracture surface energy. As in the case with spherical indentors, it is again noted that there is little difference between lubricated and non-lubricated contacts.

Equation 21 relies on the value of $\phi_a$, which has been determined from the calculated stress field for frictionless contact between the indentor and the specimen. The high values of fracture surface energy implied in our experimental results provides our justification for the inclusion of the factor $\beta$ in Equation 22. Further, the value chosen for $\phi_a$ at the plateau, which also influences the estimate of $\gamma$, is to some extent a matter of individual judgement. Any error in estimating $\phi_a$ can also be absorbed by $\beta$. Even though we observe little difference in fracture loads between lubricated and non-lubricated contact for abraded specimens for both spherical and cylindrical indentors, we find that

this is not the case for tests on as-received specimens. We discuss the significance of β and the effect of contact friction in Section 6.

Equation 22, with the exception of the factor β, is a description of the energy balance model proposed by Mouginot and Maugis, and we are not concerned with the calculation of the probability of fracture until we consider the mean fracture loads in the next section.

### 5.2.2. Median fracture load

In an attempt to explain Auerbach's Law, some workers have correlated the values of scatter in the fracture loads with the surface flaw characteristics of the specimen to arrive at a relationship between the median fracture load and indentor radius. For example, Oh and Finnie [12] initially determined Weibull parameters from bending tests on glass strips. The probabilities of failure for annular regions surrounding the indentor were calculated upon the basis of a non-diminishing stress field and combined to give a total probability of failure. From these results, the expected value of the fracture load for a given indentor size was calculated and compared with the mean fracture load obtained from indentation experiments. In a similar series of experiments, Hamilton and Rawson [5] determined the Weibull parameters which best described indentation fractures.

Fig. 10a shows the mean fracture loads for spherical indentors on as-received surfaces as reported in various literature sources [5, 12, 13] as well as the experimental results of the present work. It is evident that the slopes of the data sets shown in Fig. 10a are very different. The mean fracture loads obtained in the experiments of the present work, on as-received float-glass, are very similar to those obtained by Hamilton and Rawson [5] for the "free" side of their float glass specimens. These workers found that the tin side of their specimens was significantly weaker than the free side, as would be expected for a surface which has suffered some abrasion during manufacture. As noted above, no such difference was observed in our measurements. Evidently, the float glass used in the present work did not suffer the same type of damage during manufacture and handling as that used by Hamilton and Rawson.

For the abraded glass, our experimental results for as-received specimens show a somewhat higher mean fracture load than those obtained by Langitan and Lawn. It should be noted, however, that Langitan and Lawn used plate glass, which probably contains a significantly higher density of flaws, especially in the as-received condition, due to its method of manufacture. This is in accordance with the results of Hamilton and Rawson [5] who found that the slope of a plot of $\log P$ versus $\log R$ in the Auerbach range was sensitive to changes in surface condition. The results of Oh and Finnie [12], who used borosilicate glass, show substantially lower mean fracture loads for all indentor radii and we discuss the significance of this shortly. It should be finally noted that there is little difference between the slope of the lines of best fit to the experimental data from the present work for lubricated and non-lubricated contact.

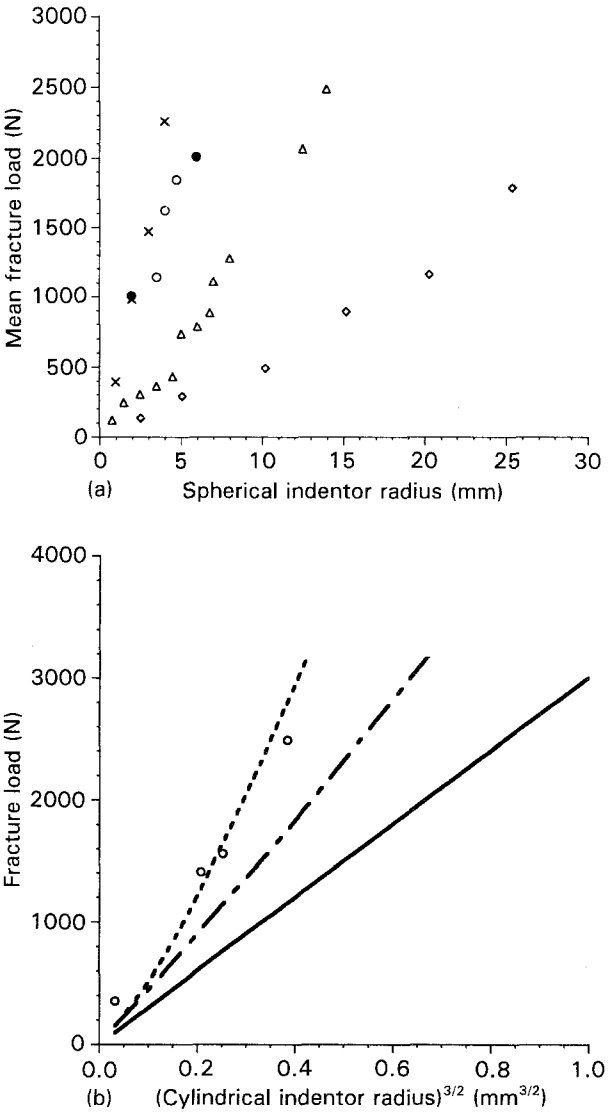


*Figure 10* Mean fracture load versus indentor radius for as-received glass. Results from the present work are shown for non-lubricated and lubricated contact. Also shown are the results obtained from various literature sources for similar experimental conditions: (a) spherical indentors; (b) cylindrical indentors. Also shown in (b) are the calculated mean fracture loads for (– – –) as-received and (— — —) weathered glass based upon $\gamma = 3.6\,\mathrm{J\,m^{-2}}$, $\beta = 2.5$ and also (——) the calculated minimum critical load $P_a$. (a) (●) Experiment, as-received, lubricated soda–lime float; (○) experiment, as-received non-lubricated soda–lime float; (×) [5], as-received borosilicate; (◇) [12], as-received borosilicate; [13], as-received soda–lime plate. (b) (○) Experiment, mean load, as-received soda–lime float.

Although the theory predicts that, within the Auerbach range there is a linear relationship between the minimum critical load and the indentor radius, there is no particular reason why this should be so for median or mean fracture loads. Indeed, if a linear relationship were to exist, it would be expected that the Auerbach constants obtained from such data would be largely determined by the flaw statistics of the sample, rather than by the intrinsic properties of the materials.

Experimental data for fracture load using lubricated cylindrical indentors on as-received soda–lime glass are shown in Fig. 10b. As noted above, conical fractures could not be obtained with non-lubricated cylindrical indentors on as-received specimens. Fig. 10b also shows calculated values for the minimum critical load, and the mean fracture loads for both weathered

and as-received glass using cylindrical indentors. The calculated curves were obtained using a value for $\beta = 2.5$. This was found to give good agreement with the experimental data for lubricated contact on as-received glass, and also reflects the difference in apparent surface energies implied by the data in Fig. 9a and b. Although our use of the scaling parameter $\beta$ is somewhat empirical, it does serve to quantify the degree of interfacial friction, at least to a first approximation. The validity of this procedure can be more fully appreciated with reference to Figs 11 and 12.

In Fig. 11 we have plotted the spread of fracture loads for as-received soda–lime glass for one particular cylindrical indentor with lubricated contact. Fig. 11 shows that most fractures occur at a load several times greater than the minimum fracture load,

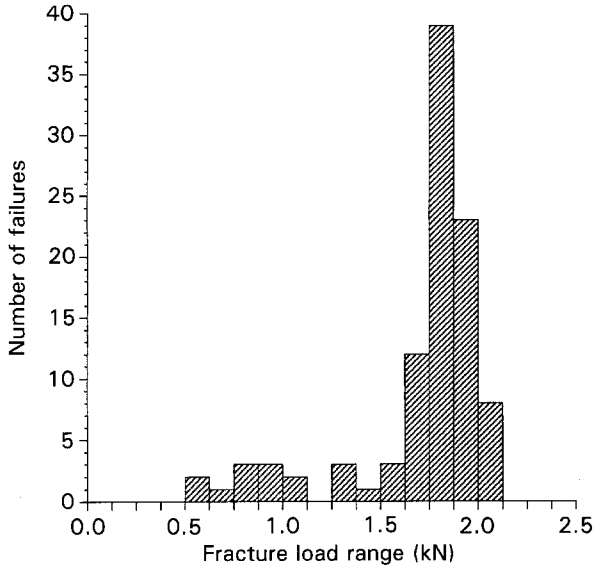


*Figure 11* Histrogram of number of failures versus fracture force from experimental data on as-received glass for a lubricated cylindrical indentor of radius 0.4 mm.

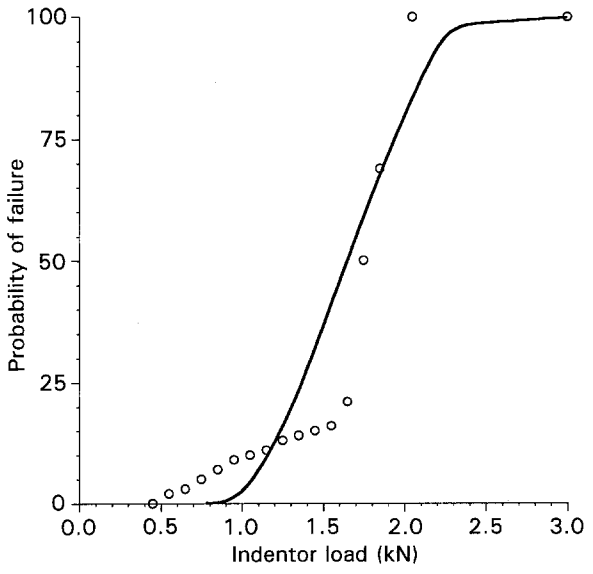


*Figure 12* Cumulative histogram showing probability of failure for a cylindrical indentor, radius 0.4 mm, from (○) experimental data, together with (——) the calculated probability of failure for as-received glass assuming $\gamma = 3.6\,\mathrm{J\,m^{-2}}$ and $\beta = 2.5$, $m = 7.3$, $k = 5.1 \times 10^{-57}$.

but there is a significant number of fractures for intermediate loads. The data of Fig. 11 are re-plotted in Fig. 12 as a cumulative distribution which is normalized to give the probability of failure. Also shown in Fig. 12 is the calculated probability of failure obtained from the method previously described in Section 4. the calculated curve shown in Fig. 12 uses the same value for $\beta$ as in Fig. 10b.

We discuss the significance of the results presented in Figs 10b, 11 and 12 in the next section. However, it should be noted at this point that the calculated values of mean fracture loads use surface strength parameters, $m$ and $k$, obtained by Brown from a fit to a range of fracture data from experiments conducted with both plate and sheet glass. The sizes of the flaws which initiate fracture in indentation tests are generally much less than those sampled in bending failure tests. The validity of our calculated results depends upon whether the extrapolation to smaller flaw sizes, inherent in the Weibull statistics assumed in Equation 23, is appropriate.

## 6. Discussion

The results of our finite-element calculations and our experimental observations raise important questions about the role of slip in establishing a classical Hertzian stress field within a specimen loaded by a cylindrical indentor. Theoretical treatments of Hertzian fracture have traditionally assumed a condition of full slip. Argon *et al.* [18] show that the mean fracture load for tests with spherical indentors and lubricated contact do not differ greatly compared with the mean fracture load obtained with non-lubricated contacts. However, Johnson *et al.* [9] propose that Argon *et al.* did not achieve a condition of full slip with their apparatus and report that, due to elastic mismatch between indentors and specimens possessing different elastic properties, mean fracture loads up to 50% higher are obtained when the indentor is more rigid than the specimen. Spence [19] provides a mathematical description of the phenomenon, for both cylindrical and spherical indentors, which proposes an inner circle of adhesive contact surrounded by an annular region where the degree of slip is determined by the coefficient of friction at the interface.

Our finite element calculations, for a cylindrical indentor, show that the indentation stress field is significantly modified when the indentor is securely bonded to the specimen – a condition of no slip. Our experimental work shows that although for abraded specimens there was little difference between the fracture loads for lubricated and non-lubricated contact, a considerable difference was noted for cylindrical indentors on as-received glass. This is not surprising, because for abraded specimens, contact is no doubt occurring via the asperities associated with the roughness of the specimen surface. For an as-received surface, the lubricant would be more uniformly spread across the contact surface leading to a lower overall level of friction. This may not be the case for spherical indentors where the geometry may lead to quite different levels of friction.

The value of fracture surface energy $\gamma = 17\,J\,m^{-2}$ for soda–lime glass implied by the data shown in Fig. 9b, and using Equation 21, is considerably larger than the predicted value of $3.6\,J\,m^{-2}$. However, the value for $\phi_a$ in Equation 21 assumes a stress field associated with a condition of full slip. If, in fact, only partial slip actually occurs during indentation experiments, then the results of the finite element work suggest that a larger force would be required to produce stress levels capable of initiating fracture. Thus, although Equation 21 may be used to estimate changes in fracture surface energy, it may not be a reliable estimate of its absolute value, because even with lubricated contact, a condition of full slip cannot be guaranteed.

The predicted fracture surface energy of borosilicate glass, $\gamma = 5.2\,J\,m^{-2}$, is higher than that of soda–lime glass, $\gamma = 3.6\,J\,m^{-2}$. However, it is interesting to note that both Mouginot and Maugis [7], and Oh and Finnie [12] obtained consistently lower fracture loads for borosilicate glass compared to the results of the present work and that of Langitan and Lawn for soda–lime glass for similar sized indentors. We may possibly infer, therefore, that there is inherently more friction associated with soda–lime glass than with borosilicate glass. The data of Figs 9 and 10 imply that the presence of friction raises the fracture forces by a factor of approximately 2.5 as implied by our choice of the factor $\beta$ in Equation 22. This is in qualitative agreement with the findings of Johnson *et al.* [9] who, as previously mentioned, observed increases in fracture loads of up to 50% under certain conditions of elastic mismatch between the indentor and the specimen.

A full treatment of interfacial slip is beyond the scope of the present work. Our purpose in this work is to demonstrate a method whereby the probability of obtaining a Hertzian cone crack may be calculated if the specimen surface can be characterized by the Weibull strength parameters, $m$ and $k$. Experimental evidence shows that in order to achieve this goal, a precise knowledge of the indentation stress field is required and this is influenced by the presence of friction. We propose that this may be done in the first instance by the factor $\beta$ in Equation 22. Further experimental work should be done to investigate the role of slip. For surfaces with a low density of flaws, both slip and the presence of flaws influence the mean fracture load. These two effects could be separated by conducting tests with a cylindrical indentor where the specimen surface was abraded only outside the contact area. This would indicate whether or not the level of tensile stress was indeed sufficient to initiate a cone crack. Alternately, the surface stresses near the contact could be measured directly using strain gauges.

Workers who have attempted to apply flaw statistical methods to explain Auerbach's law have done so without considering the diminishing stress field in the vicinity of the indentor. Oh and Finnie [12] use surface flaw parameters obtained from bending tests but apply them incorrectly, using only the surface stress levels in the Weibull formula. Hamilton and Rawson [5] determine surface flaw strength parameters which describe the variation of the median fracture load but again do so in terms of the surface stresses. The energy balance approaches of Frank and Lawn, and Mouginot and Maugis show that the diminishing stress field is a key feature of the phenomenon. The present work describes how flaw statistics may be combined with energy balance arguments to give a more complete treatment of the problem.

It is clear from the present work that the value of the Auerbach constant depends upon the specimen surface condition. There appears to be considerable confusion in the literature about whether Auerbach's law refers to mean, median or minimum fracture loads. Indeed, Auerbach's original paper [3] gives only scant mention to the linear relationship between indentor load and radius. The present work shows that there is no particular reason why there should be this linear relationship for median or mean fracture loads for surfaces which do not contain a large density of flaws. We are led to conclude that, although the explanation of Auerbach's law has its origins in the energy balance theories of Frank and Lawn, and Mouginot and Maugis, the actual value of the Auerbach constant for mean fracture loads is influenced by the surface flaw statistics of each specimen. Further, Auerbach's law in the strictest sense only applies to well-abraded specimens.

We have used surface-flaw parameters determined by bending of large sheets of glass to predict the probability of the occurrence of indentation fracture. Such bending tests involve the breakage of large areas of glass which are simply supported and loaded uniformly in a normal direction with air pressure. Because large areas are used, it is reasonable to suppose that much of the data obtained preferentially include failures due to larger sized flaws. In contrast, in an indentation stress field, large flaws do not generally lead to fracture. In addition, the highly stressed area is so small that, on average, the more numerous smaller flaws will normally initiate fracture. Indentation fracture tests, therefore, preferentially sample smaller sized flaws than bending tests. Hamilton and Rawson [5] note this point but incorrectly state that this prevents indentation failure from particularly large flaws. Hu *et al.* [20] find that a small specimen size, in three-point bending tests, leads to a decrease in the measured values of the Weibull modulus, $m$. In indentation work, the Auerbach range of flaw sizes for a typical indentor with a contact radius of 0.5 mm is about 0.01–0.055 mm. Experiments with large area plates [16, 17] imply that many failures result from flaw sizes of around 1 mm for weathered glass and 0.3 mm for as-received glass, an order of magnitude larger than the flaws associated with indentation failure.

In Figs 11 and 12, we have focused our attention on one particular indentor size and compared the probability of failure predicted by the theory to that found by experiment for as-received glass. Reasonably good agreement is obtained. However, the experimental evidence at the lower load range suggests that the surface of our as-received specimens does not contain a distribution of flaw sizes which corresponds to a Weibull distribution. This is shown by existence of

failures within the lower load range. We conjecture that there may indeed be two surface flaw distributions each of which may be described by Weibull statistics. We do not pursue this idea further in the present work. The lower limit to the fracture load corresponds closely to that predicted by the theory. This is expected because the lower limit to the fracture load is independent of the surface flaw statistics of the specimen.

This work demonstrates that the finite element method can be used to calculate the indentation stress field associated with a cylindrical indentor. For a condition of full slip, inwards movement of material beneath the indentor causes the surface of the specimen just outside the contact area to be placed in tension. This tension is characteristic of the Hertzian indentation stress field. If this inwards movement of material is restricted, by frictional forces generated by adhesive contact between the indentor and the specimen, then the level of tensile stress is significantly reduced.

It should be noted that the flaw size in this terminology refers to the flaw depth, not its length along the surface. Throughout this work, we have always assumed circular symmetry. Evidently a more complete analysis of the problem will include the growth of a surface flaw into a circular ring. Our experimental work shows that the growth from a flaw into a ring is by no means instantaneous.

In the present work we have considered flaws sizes as if they were always sharp and oriented normally to the applied stress. In practice, there are considerable variations to these parameters. It is convenient to assign an equivalent flaw size to the actual flaw size within a specimen. A size equivalent to a penny-shaped, perpendicularly oriented sharp flaw may be included via a geometry correction factor in Equation 9. In this work, we have not applied such a correction because the energy balance analysis has always assumed circularly symmetric flaws which surround the indentation site, an obvious over-simplification. However, the surface flaw parameters $m$ and $k$ are indirectly related to flaw sizes through Equations 9 and 22.

## 7. Conclusion

We have shown that flaw statistics plays an important role in determining the indentation fracture strength of brittle solids. We have reviewed both the energy balance and flaw statistical explanations of Auerbach's law. A novel application of Weibull statistics has permitted the determination of the mean fracture load for a given indentor and specimen surface condition.

Indentation experiments were conducted on soda–lime float glass and compared with the predictions of the theory and the data of previous workers in this field. We have shown that although the explanation of Auerbach's law has its origins in the application of Griffith's energy balance criterion for crack growth, the actual value of the Auerbach constant for a particular specimen is influenced by its surface flaw statistics. Further, Auerbach's law in the strictest sense only applies to well-abraded specimens. The importance of slip between the indentor and the specimen has been highlighted using both experimental and finite element modelling methods. This work shows that the indentation strength of brittle solids which do not contain a high density of flaws may be substantially higher than that implied by previously published indentation test data.

## Acknowledgements

The technical assistance of H. Haldane is gratefully acknowledged. The authors thank the Department of Mechanical Engineering, University of Sydney, for use of their Instron testing machine, and M.V. Swain for useful discussions. This work was supported in part by His Royal Highness Prince Nawaf bin Abdul Aziz of the Kingdom of Saudi Arabia through the Science Foundation for Physics at the University of Sydney, and by the Australian Energy Research and Development Corporation.

## References

1. H. HERTZ, *J. Reine Angew. Math.* **92** (1881) 156; translated and reprinted in English in "Hertz's Miscellaneous Papers" (Macmillan, New York, 1896) Ch. 5.
2. *Idem., Verhandlungen des Vereins zur Beforderung des Gewerbe Fleisses* **61** (1882) 449; translated and reprinted in English in "Hertz's Miscellaneous Papers" (Macmillan, New York, 1896) Ch. 6.
3. AUERBACH, *Ann. Physik (Leipzig)* **43** (1891) 61.
4. A. A. GRIFFITH, *Phil. Trans. R. Soc.* **A221** (1920) 163.
5. B. HAMILTON and R. RAWSON, *J. Mech. Phys. Solids* **18** (1970) 127.
6. F. C. FRANK and B. R. LAWN, *Proc. R. Soc.* **A229** (1967) 291.
7. R. MOUGINOT and D. MAUGIS, *J. Mater. Sci.* **20** (1985) 4354.
8. W. WEIBULL, "A Statistical Theory of the Strength of Materials", Handlinger Nr 151 (Ingenious Vetenskaps Akademins, Stockholm, 1939).
9. K. L. JOHNSON, J. J. O'CONNOR and A. C. WOODWARD, *Proc. R. Soc.* **A334** (1973) 95.
10. G. R. IRWIN, in "Handbuch der Physik" **6** (Springer, Berlin 1958) p. 551.
11. S. W. FREIMAN, T. L. BAKER and J. B. WACHTMAN Jr, in "Strength of Inorganic Glass", edited by C. R. Kurkjian (Plenum Press, New York, 1985) p. 597.
12. H. L. OH and I. FINNIE, *J. Mech. Solids* **15** (1967) 401.
13. F. B. LANGITAN and B. R. LAWN, *J. Appl. Phys.* **40** (1969) 4009.
14. I. A. SNEDDON, *Proc. Camb. Philos. Soc.* **42** (1946) 29.
15. M. BARQUINS and D. MAUGIS, *J. Mecan. Theor. Appliq.* **1** (1982) 331.
16. W. G. BROWN, "A practicable formulation for the strength of glass and its special application to large plates", Publication NRC 14372 (National Research Council of Canada, Ottawa, 1974).
17. W. L. BEASON, "A Failure Prediction Model for Window Glass", Institute for Disaster Research, Texas Tech University, Lubbock, Texas, NTIS Accession no. PB81-148421 (1980).
18. A. S. ARGON, Y. HORI and E. OROWAN, *J. Am. Ceram. Soc.* **43** (1960) 86.
19. D. A. SPENCE, *J. Elast.* **5** (1975) 297.
20. X.-Z. HU, B. COTTERELL and Y.-W. MAI, *Philos. Mag. Lett.* **57**(2) (1988) 69.

*Received 14 June*
*and accepted 1 November 1993*